

Optimizing B-spline surfaces for developability and paneling architectural freeform surfaces

Konstantinos Gavril^{a,b,*}, Alexander Schiftner^b, Helmut Pottmann^{a,c}

^a*Applied Geometry, Institute of Discrete Mathematics and Geometry,
Vienna University of Technology, Wiedner Hauptstrasse 8-10/104, A-1040 Vienna, Austria*

^b*Evolute GmbH, Schwindgasse 4/10, 1040 Vienna, Austria*

^c*Visual Computing Center, KAUST, Thuwal 23955-6900, Saudi Arabia*

Abstract

Motivated by applications in architecture and design, we present a novel method for increasing the developability of a B-spline surface. We use the property that the Gauss image of a developable surface is 1-dimensional and can be locally well approximated by circles. This is cast into an algorithm for thinning the Gauss image by increasing the planarity of the Gauss images of appropriate neighborhoods. A variation of the main method allows us to tackle the problem of paneling a freeform architectural surface with developable panels, in particular enforcing rotational cylindrical, rotational conical and planar panels, which are the main preferred types of developable panels in architecture due to the reduced cost of manufacturing.

Keywords: developable surface, spline surface, architectural geometry, computational differential geometry, constrained optimization

1. Introduction

Developable surfaces can be locally mapped to a planar domain without distortion. Since they can be constructed from an initial planar state without stretching or tearing, only by bending, they represent the shapes obtainable with thin materials like sheet metal or paper which do not stretch. These surfaces are of great interest to many applications. Areas like architecture, manufacturing and design take advantage of the cost-reduced manufacturing process that developables have.

Developable surfaces have been well studied in classical differential geometry. Developable, twice differentiable surfaces are *single curved*, meaning one of the principal curvatures is zero. Thus, the Gauss curvature vanishes at every point. They are composed of special *ruled* surfaces with a constant tangent plane at all points of a ruling. As the surface normal vectors along a ruling agree, the Gauss image of a developable surface is 1-dimensional, i.e. a curve.

We base the main method in our paper on this property of the Gauss image. However, our focus is not on exact developability, but rather on *nearly developable* surfaces which we characterize by nearly curve-like Gauss images. The motivation for our research is the fact that most materials allow for a little bit of stretching and therefore developability needs not be satisfied to a high degree in a variety of applications. In particular, we are interested in applications in architecture where various kinds of tolerances can be exploited to reduce the production cost of freeform skins. Our work fits into a larger research program on novel digital tools which consider key aspects of function and fabrication, including material behavior, already in the early design and digital modeling phase.

Previous work. There is a vast amount of literature on developable surfaces, on their theory, their computational design using various types of representations and on their appearance in numerous applications. We limit this discussion to three main areas which are most closely related to our work: (i) developable Bezier and B-spline surfaces, (ii) discrete representations and nearly developable surfaces and (iii) their importance in paneling architectural surfaces.

*Corresponding author

Email addresses: gavril@evolute.at (K. Gavril), schiftner@evolute.at (A. Schiftner), pottmann@geometrie.tuwien.ac.at (H. Pottmann)

Developable Bezier and B-spline surfaces. Lang and Röschel [1] expressed developability of rational, in particular polynomial Bézier surfaces in a system of cubic equations. In general, this system cannot be solved in a simple way, but in various special cases, explicit solutions have been derived ([2, 3, 4, 5]). One can avoid these nonlinear constraints by using the projectively dual representation, where a developable is represented as the envelope of its tangent planes. For details, we refer to [6, Section 6.2], but note that the dual representation is not sufficiently intuitive to be suitable for interactive design. Moreover, it is difficult to control singularities. A combination of the primal and the dual representation has been successfully employed for interactive design of developable NURBS surfaces by Tang et al. [7].

Discrete representations and nearly developable surfaces. There are numerous papers which model developable surfaces with triangle meshes; we just refer to a few of them [8, 9, 10, 11]. Jung et al. [12] improve on Decaudin et al.’s [13] method that locally approximates neighborhoods around each mesh triangle with a cone. Liu et al. [14] treat developable surfaces as a limit case of meshes from planar quads. Solomon et al. [15] use a mesh approach to flexibly model the shapes achievable by bending and folding a given planar domain without stretching or tearing. An elegant discrete model of developable surfaces is provided by special quad meshes which discretize orthogonal nets of geodesics [16, 17].

Nearly developable surfaces appear in connection with specific applications, e.g. modeling ship hulls [18] and clothing [19] or segmenting meshes in geometry processing [20, 21]. Narain et al. [22] go beyond developability and present a technique for simulating plastic deformation in sheets of thin materials, such as crumpled paper, dented metal, and wrinkled cloth. Closely related to our work is a paper by Wang et al. [23] on increasing developability of a trimmed NURBS surface, but our approach and applications differ significantly.

Another very recent work with a strong connection to our research is the developable surface flow by Stein et al. [24]. This flow is a gradient flow on the energy $\int_M \kappa_1^2 dA$, κ_1 being the smallest principal curvature. It constructs piecewise developable rather than globally developable surfaces as minimizers. The discrete model is based on triangulations whose vertex stars dominantly lie in pairs of planes. One could say that the surface is locally approximated by a pair of planes, their intersection representing the ruling direction. In a similar spirit, our local approximations are of higher order, as discussed below. Note that Stein et al. generate *piecewise* developable surfaces, where the arising pattern of developable patches is a result of the geometric flow and depends on the initial triangulation. We can increase developability of a single smooth surface without the introduction of tangent discontinuities. We can also allow for piecewise developable surfaces through an appropriate selection of knots and their multiplicities in the underlying B-spline surface, but our arrangements of developable patches are more restricted (and at the same time more controlled) than the ones by Stein et al.

Paneling architectural surfaces. Architectural surfaces need to be decomposed into panels, which is a key process and largely responsible for a cost effective solution. For an overview of the problems in this field we refer to [25]. In particular, we point to the paneling solution of Eigensatz et al. [26]. It exploits various tolerances at seams and a cost model for the production of panels of different geometric types to suggest solutions within an optimization framework. The user provides the design surface and a suggested network of panel boundary curves, while the algorithm slightly adapts the design surface and network and optimally fills it with panels (patches). Our work can be considered as an extension in the sense that the panel boundaries are also subject to optimization with the overall goal of increasing developability of the individual panels. For developable and nearly developable surfaces in architecture, we further point to [27, 28, 29, 30].

Contributions. The main contributions of this paper are as follows:

- We present a novel optimization method for increasing the developability of an arbitrary surface. It is based on local approximations of the surface by developable surfaces with planar and thus circular Gauss images. While we could also use other representations within our framework, we prefer B-splines in order to have simple access to smoothness of patches. Moreover, we naturally obtain a patchwork of regular quad combinatorics, which is a preferred arrangement in many architectural projects.
- We provide a justification of our approach in two ways: We discuss local approximations of developable surfaces, especially with those being characterized by a planar Gauss image. Moreover, we study the implications of a nearly curve-like Gauss image on the underlying

surface, thus supporting our claim of achieving near developability through Gauss image thinning.

- We introduce a variation of the main method presented in the paper to tackle the problem of paneling a freeform surface with (rotational) cylindrical, (rotational) conical and planar panels, which are the main preferred types of developable panels in architecture due to the reduced cost of manufacturing.
- We provide results that illustrate the power of the proposed approach and outline potential directions for future research.

Overview of the paper. This paper is organized as follows. In Section 2, we outline some important fundamentals for our work and, in section 3 present the main optimization algorithm step by step. Section 4 focuses on a variation of the main optimization algorithm which is designed for paneling a freeform surface with panels that are special cases of developable surfaces. We present the differences with the main algorithm and introduce any necessary new tools. In section 5, we provide results on various data sets, including ones from real architectural projects. Moreover, we discuss advantages and shortcomings of our approach and outline future work.

2. Fundamentals

2.1. Local approximations of developable surfaces

We are interested in smooth or piecewise smooth developable surfaces S . They are composed of C^2 surface patches which fall into one of the following four categories: planes, general cylinders, general cones and tangent surfaces of space curves. Their *Gauss images* C , i.e. sets of unit normals viewed as points on the unit sphere S^2 , are composed of *curves*. The junction points of C where more than two curve segments meet, correspond to planar patches on S . In the following, we discuss only the three non-trivial basic types: These are ruled surfaces with a constant tangent plane along each ruling. In other words, they are envelopes of a one-parameter family of planes.

We are interested in second order local approximations of these basic types. The following result is well-known (see, e.g. [6, Theorem 6.1.4]) and closely related to the simple fact that the Gauss image of a developable surface is a spherical curve, which has an osculating circle at each of its regular points.

Lemma 2.1. *Along each ruling r , a non-planar developable ruled surface S has second order contact with a rotational cone Γ (osculating cone). The vertex of this cone is the singular point of r (regression point). Γ is a rotational cylinder for a cylindrical ruling r (regression point at infinity) and it degenerates to a plane if r is an inflection ruling.*

Let us add a bit more detail for the generic case where S is the tangent surface of a space curve, $S : \mathbf{x}(u, v) = \mathbf{c}(u) + v\dot{\mathbf{c}}(u)$. This so-called regression curve $\mathbf{c}(u)$ is a singular curve on S . The osculating plane at $\mathbf{c}(u)$, spanned by $\dot{\mathbf{c}}, \ddot{\mathbf{c}}$, is the constant tangent plane of S along a ruling (isoparameter line $u = \text{const}$). If u is an arc length parameter, then the Frenet frame at $\mathbf{c}(u)$ is given by the tangent vector $\mathbf{e}_1 = \dot{\mathbf{c}}$, principal normal $\mathbf{e}_2 = \ddot{\mathbf{c}}/\kappa$ (with curvature $\kappa = \|\ddot{\mathbf{c}}\|$), and the binormal vector $\mathbf{e}_3 = \mathbf{e}_1 \times \mathbf{e}_2$. The Frenet equations can then be written in the form $\dot{\mathbf{e}}_i = \mathbf{d} \times \mathbf{e}_i$. Here $\mathbf{d} = \tau \mathbf{e}_1 + \kappa \mathbf{e}_3$ is the so-called Darboux vector, where τ denotes the torsion. The Darboux vector is the direction vector of the osculating cone Γ . This means that the angle ϕ between cone axis and ruling satisfies $\cot \phi = \tau/\kappa =: k$, a value which is called *conical curvature* of the developable surface at the ruling.

The Gauss image of a rotational cone Γ is a circle C on S^2 which becomes a great circle if Γ is a cylinder and degenerates to a point for a plane Γ . So all 2nd order local approximations addressed above have a *planar Gauss image* curve C . However, a planar Gauss image C of a surface Γ does not yet imply that Γ is a cone, while Γ must be a cylinder if C is a great circle and a plane if C is just a point. So let us discuss the case of a small circle C as Gauss image of a surface. These surfaces are well studied in classical differential geometry and known as *surfaces of constant slope*. They are the tangent surfaces of curves c of constant slope. Their tangents form a constant angle with a certain direction in space, which is obviously the rotational axis of the circle C . For a detailed study of these surfaces, we refer to [6, Section 6.3]. The increased degrees of freedom compared to the osculating cone allow us to increase the local approximation of an arbitrary developable surface by one with a planar Gauss image:

Theorem 2.2. At each regular point p of a developable ruled surface S , there is a developable surface Γ with a planar Gauss image, which has second order contact with S along the entire ruling through p and interpolates a curve $a \subset S$ through p .

Proof. We omit the cases where S is a plane or a cylinder, since these surfaces already have a planar Gauss image curve. So we are left with cones and tangent surfaces S . We pick the osculating cone Γ_p of S along the ruling r_p through p and intersect S with the plane A through p which is orthogonal to the axis of Γ_p . This yields the curve a . Note that the plane A intersects the cone Γ_p in a circle, which is the osculating circle of a at p . The construction of the developable surface Γ proceeds as follows: Through each tangent of a we compute the two planes which form the same angle with the axis of Γ_p as Γ_p does. Among these two planes, we select the one which is closer to the corresponding tangent plane of S . Then, the envelope of this family of planes is the desired developable surface Γ with a planar Gauss image described in the theorem. By construction, Γ and S share the osculating cone Γ_p and thus have second order contact along the ruling through p . We could choose another curve $a \subset S$ which lies transversal to the rulings of S , but leave it with this special choice as it simplifies the further analysis.

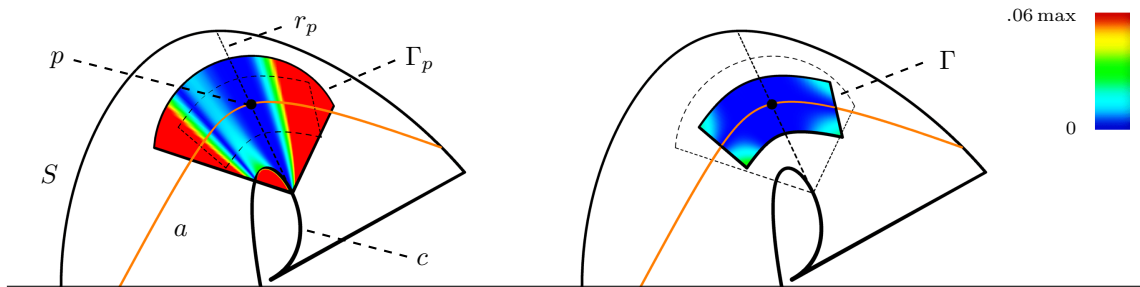


Figure 1: Local approximations of a developable surface S , which is the tangent surface of a space curve c . Left: The osculating cone Γ_p at a point $p \in S$ approximates S to 2nd order along the entire ruling r_p . Right: A developable surface Γ as in Theorem 2.2 approximates S even better, as is seen from the color coding of Γ and Γ_p according to their orthogonal distance to S .

For that, we use a local (x, y, z) coordinate system with $A : z = 0$ and describe the curve a by its support function $h(u)$. This means that we view a as envelope of its tangent lines

$$L(u) : x \cos u + y \sin u + h(u) = 0,$$

which form the angle u with the y -axis and possess the signed distance $h(u)$ from the origin (if the positive side of L is determined by the normal vector $(\cos u, \sin u)$). The derivative with respect to u is the curve normal, $\dot{L}(u) : -x \sin u + y \cos u + \dot{h}(u) = 0$. Intersecting the two lines L, \dot{L} , we obtain a parameterization of the curve a as

$$\mathbf{a}(u) : x = -h \cos u + \dot{h} \sin u, \quad y = -h \sin u - \dot{h} \cos u.$$

Differentiating again yields the curvature centers (evolute) of $\mathbf{a}(u)$ as $\mathbf{a}^*(u) = \dot{\dot{L}} \cap \ddot{L}$,

$$\mathbf{a}^*(u) : x = \dot{h} \sin u + \ddot{h} \cos u, \quad y = -\dot{h} \cos u + \ddot{h} \sin u.$$

Thus, the signed curvature radius of $\mathbf{a}(u)$ is $\rho(u) = h(u) + \ddot{h}(u)$.

Let p be the point $\mathbf{a}(0) = (-h(0), -\dot{h}(0), 0)$. To shorten notation, we use the notation $h(0) =: h_0$ and likewise for the derivatives. Then the z -parallel line through the curvature center $\mathbf{a}^*(0) = (\ddot{h}_0, -\dot{h}_0, 0)$ is the axis of the osculating cone Γ_p . With k as conical curvature of Γ_p and of S at $u = 0$, the vertex of Γ_p has z -coordinate $z = (h_0 + \ddot{h}_0)/k = \rho_0/k$. Planes $P(u)$ through the tangents of \mathbf{a} and with the same inclination against the z -axis as Γ_p have the equations

$$P(u) : x \cos u + y \sin u - kz + h(u) = 0. \tag{1}$$

Their envelope is the desired approximation Γ of S at p with a planar Gauss image and through \mathbf{a} . Differentiating with respect to u yields planes \dot{P}, \ddot{P} whose equations agree with those of \dot{L}, \ddot{L} and are therefore z -parallel planes through these lines. Recall that rulings of Γ are obtained as

intersections $P \cap \dot{P}$ and the regression curve is found as $P \cap \dot{P} \cap \ddot{P}$. As discussed in more detail in [6, Section 6.3], the regression curve of Γ lies in the z -parallel cylinder through \mathbf{a}^* and the intersections of Γ with planes $z = \text{const}$ are translated offsets of \mathbf{a} . The intersection curve \mathbf{a}_1 of Γ with the plane $z = 1$ is a translated version of the offset of \mathbf{a} at distance k and therefore has a support function $h(u) - k$. The ruling vectors $\mathbf{r}_1 = \mathbf{a}_1 - \mathbf{a}$ of Γ are $\mathbf{r}_1(u) = (k \cos u, k \sin u, 1)$.

The intersection curve $\bar{\mathbf{a}}$ of S with $z = 1$ has a support function $\bar{h}(u) = h(u) - k + f(u)$. Due to the 2nd order contact at $u = 0$, we have $f(0) = \dot{f}(0) = \ddot{f}(0) = 0$. Then, the tangent planes of S are

$$T(u) : x \cos u + y \sin u + (f(u) - k)z + h(u) = 0, \quad (2)$$

and the ruling vectors of S are $\mathbf{r} = \bar{\mathbf{a}} - \mathbf{a}$,

$$\mathbf{r}(u) = ((k - f) \cos u + \dot{f} \sin u, (k - f) \sin u - \dot{f} \cos u, 1).$$

Now we have parameterizations of S as $\mathbf{s}(u, v) = \mathbf{a}(u) + v\mathbf{r}(u)$ and of Γ as $\mathbf{g}(u, v) = \mathbf{a}(u) + v\mathbf{r}_1(u)$, which concludes the proof.

However, we want to go beyond that and estimate the distance between S and its approximation Γ , and compare it to the distance between S and the osculating cone Γ_p .

We over-estimate the distances by measuring them in planes $z = \text{const} = v$ and there between points with parallel tangents. This means that we measure distances between points of the two surfaces which have the same parameter values (u, v) . This distance $\delta(u, v)$ between S and Γ is given by

$$\delta(u, v) = |v| \|\mathbf{r}_1(u) - \mathbf{r}(u)\| = |v| \sqrt{f(u)^2 + \dot{f}(u)^2}. \quad (3)$$

We can also look at distances $\bar{\delta}$ between the parallel tangents directly, which are in view of equations (1) and (2),

$$\bar{\delta}(u, v) = |vf(u)|.$$

For $u = 0$ we get the ruling r_p through p and of course $\delta, \bar{\delta} = 0$.

Let us compare this with the approximation of S by the osculating cone Γ_p . The cone is given by (1) where h is replaced by the support function h_c of the osculating circle \mathbf{c}_o of \mathbf{a} at $p = \mathbf{a}(0)$,

$$h_c(u) = \rho_0 + \dot{h}_0 \sin u - \ddot{h}_0 \cos u.$$

The parameterization of the osculating circle is

$$\mathbf{c}_o(u) = (\ddot{h}_0 - \rho_0 \cos u, -\dot{h}_0 - \rho_0 \sin u, 0).$$

Thus, a parameterization of Γ_p is given by $\mathbf{c}_o(u) + v\mathbf{r}_1(u)$, and the two errors $\delta_p, \bar{\delta}_p$ between S and Γ_p become

$$\delta_p(u, v) = \|\mathbf{c}_o(u) - \mathbf{a}(u) + v(\mathbf{r}_1(u) - \mathbf{r}(u))\|, \quad \bar{\delta}_p(u, v) = |vf(u) + h(u) - h_c(u)|.$$

To get better insight into the behavior of the errors, we insert Taylor expansions at $u = 0$,

$$f(u) = a_3 u^3 + \dots, \quad h(u) = h_0 + \dot{h}_0 u + \frac{\ddot{h}_0}{2} u^2 + \frac{\ddot{\ddot{h}}_0}{3} u^3 + \dots$$

The error vector between \mathbf{a} and \mathbf{c}_o now reads

$$\mathbf{c}_o(u) - \mathbf{a}(u) = \left(-\frac{\dot{\rho}_0}{3} u^3 + \dots, \frac{\dot{\rho}_0}{2} u^2 + \frac{\ddot{h}_0}{6} u^3 + \dots, 0\right).$$

Note that the quadratic term in the error vector is in tangential direction at p , and thus confirms the 2nd order contact between $\mathbf{c}_o(u)$ and $\mathbf{a}(u)$ at p . For the errors, we find the following expansions,

$$\delta(u, v) = |3a_3 u^2 v + \dots|, \quad \bar{\delta}(u, v) = |a_3 u^3 v + \dots|,$$

and

$$\delta_p(u, v) = \left|\frac{\dot{\rho}_0}{2} u^2 + 3a_3 u^2 v + \dots\right|, \quad \bar{\delta}_p(u, v) = \left|\frac{\dot{\rho}_0}{6} u^3 + a_3 u^3 v + \dots\right|.$$

As expected, the approximation of S by the osculating cone Γ_p is not as good as with Γ , since the deviation in the base plane $z = 0$ ($v = 0$) adds to the error everywhere. The appearance of the

derivative $\dot{\rho}_0$ of the curvature radius $\rho(u)$ at $u = 0$ in the lowest order term is no surprise, as for $\dot{\rho}_0 = 0$ the osculating circle \mathbf{c}_o has 3rd order contact with \mathbf{a} and S at p .

There is one exception which we did not cover here, namely if the ruling r_p through p is an *inflection ruling*. In that case, Γ_p degenerates to the tangent plane, and one cannot parameterize directly via the tangent directional angle u . Instead, one can use another parameter t , and work with a parameterization in support coordinates $(u(t), h(t))$, as in [6, pp. 362-363].

Knowing that surfaces with a planar Gauss image approximate developable surfaces at each point so well, we can increase developability by enforcing local approximations of this type through an optimization algorithm (see section 3).

2.2. Surfaces with a thin Gauss image

Our method will try to make the Gauss image of a B-spline surface thinner. After that, it will lie in a region R_ε on the sphere which has at most geodesic distance ε to a curve $C \subset S^2$. Let us briefly discuss the implications on a surface S which has a Gauss image in such an ε -strip R_ε . For that, we pick a part of the surface without an umbilic; there the principal curvature lines form a quadrilateral curve network without singularities. For simplicity, let us just consider a patch $\mathcal{P} \subset S$ in this region which is bounded by four principal curvature lines and does not contain parabolic points. Moreover, we select a square-like patch \mathcal{P} , meaning that the average length of the two pairs of opposite boundary curves is the same. The Gauss image $\sigma(\mathcal{P})$ of that principal patch \mathcal{P} is a principal patch on S ; corresponding curves on P and $\sigma(\mathcal{P})$ have parallel tangents at corresponding points, as they are principal directions and thus eigendirections of the derivative of the Gauss map. As we exclude parabolic points in \mathcal{P} , the Gauss map is regular everywhere and thus locally injective.

The Gauss image $\sigma(\mathcal{P})$ of \mathcal{P} is squeezed into the thin region R_ε . Being contained in R_ε , at least one family F_1 of principal curvature lines on \mathcal{P} must be mapped to very short curves in R_ε . If this is not true for the other family F_2 of principal curvature lines; the Gauss image curves of that family must be nearly parallel to the central curve C of R_ε . Thus, the Gauss images of curves in F_1 will be nearly orthogonal to C (see Figures 11, 12). Their length can be bounded depending on the width variation of $\sigma(\mathcal{P})$. The shortening of curves in F_1 through the Gauss map to a length $\approx \varepsilon$ implies that the curves themselves will be close to straight lines. A surface with one family of straight principal curvature lines is exactly developable; our surface is only an approximation of that. A more thorough investigation of the geometric implications of a thin Gauss is left for future research.

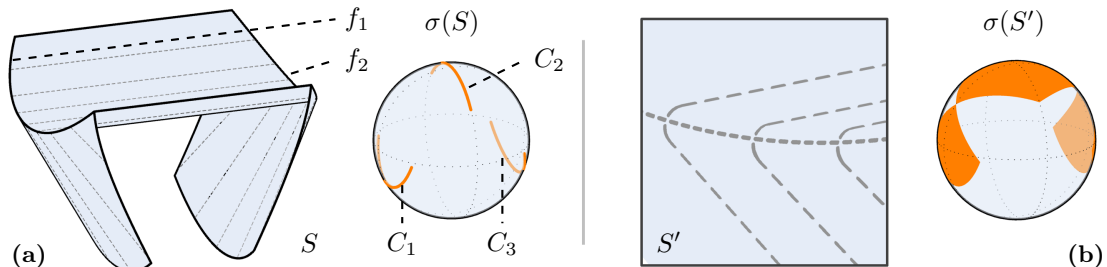


Figure 2: (a) Example of a developable shape S with curved folds f_1, f_2 , and its Gauss image $\sigma(S) = C_1 \cup C_2 \cup C_3$. (b) Rounding the fold curves of S , leads to shape S' with Gauss image $\sigma(S')$ which is not thin.

Due to our focus on architectural geometry, we can exclude surfaces with wrinkles or folds appearing for example in cloth. These wrinkles are close to curves formed by parabolic points and have one very high principal curvature. They are not of interest in the present paper, and are not characterized by thin Gauss images. Some insight into the geometry of these folds can be obtained as follows: Consider a planar sheet of material, mark a fold curve on it and bend it into a 3D shape S , leading to a developable surface with a curved crease (for the local geometry of such curved folds, see e.g. ([6, Section 6.5])). The two developable surfaces on either side of the fold curve f have curves C_1, C_2 as Gauss images. Now let us add a thin smooth blend to round off the fold curve f . The Gauss image of that blend surface will connect the two curves C_1, C_2 to a region which needs not be thin at all. With a sufficiently small blending radius the shape S can

be arbitrarily close to an exact developable surface and thus be nearly developable, but the Gauss image will not be thin (see Figure 2).

Therefore, our approach of thinning the Gauss image implies the construction of nearly developable surfaces, but the converse is not true. A nearly developable surface needs not have a thin Gauss image, due to the phenomenon of wrinkles. For materials which allow only very little stretching, these wrinkles appear to be smoothed versions of developable surfaces with curved folds, as indicated above. There is interesting research on this phenomenon, combining geometry and physics; see e.g. [31]. However, we are not aware of any differential geometric characterization of nearly developable surfaces which does not use the planar unfolding.

2.3. Developable bicubic surfaces

We will use bicubic B-spline surfaces and thus it is appropriate to justify this choice. When it comes to modeling nearly developable surfaces, our choice is natural due to the approximation power of splines. The condition of one family of nearly straight principal curvature lines is sufficiently soft to be modeled nicely with these splines.

However, especially in our architectural application, we will model panel arrangements also by bicubic B-spline surfaces, with knots of multiplicity three, which are just C^0 patchworks of bicubic polynomial patches. We want these polynomial patches to be close to developable surfaces, in particular to right circular cones or cylinders. Thus, we briefly discuss *developable bicubic surfaces*.

Bicubic patches on tangent surfaces. The tangent surface of a polynomial cubic $\mathbf{c}(u)$ can be parameterized as

$$\mathbf{x}(u, v) = \mathbf{c}(u) + v\dot{\mathbf{c}}(u),$$

and it is therefore a bicubic surface. In this form, the rulings are v -isoparameter curves and an axis aligned rectangle in the parameter domain represents a patch on the surface bounded by two rulings. There are other bicubic patches on that surface, which are obtained as images of arbitrary parallelograms in the (u, v) -plane. Equivalently, one can obtain them as images of the unit square $[0, 1]^2$ in a (\bar{u}, \bar{v}) parameter plane via an affine parameter change,

$$u = a_0 + a_1\bar{u} + a_2\bar{v}, \quad v = b_0 + b_1\bar{u} + b_2\bar{v}.$$

Furthermore, special bilinear re-parameterizations where the first equation remains and the second one reads

$$v = b_0 + b_1\bar{u} + b_2\bar{v} + b_3\bar{u}\bar{v},$$

also yield bicubic patches on that tangent surface.

Even the tangent surface of a polynomial quartic $\mathbf{c}(u)$ has a bicubic parameterization. We write $\mathbf{c} = \mathbf{a}_4u^4 + \mathbf{a}_3u^3 + \dots + \mathbf{a}_0$ in monomial form and parameterize its tangent surface as

$$\mathbf{x}(u, v) = \mathbf{c}(u) + (-u/4 + v)\dot{\mathbf{c}}(u),$$

which is a bicubic representation. A complete classification of all bicubic tangent surfaces is an open problem. For our purposes it suffices to see that tangent surfaces of quartic curves are included in this class of surfaces, which leaves sufficient flexibility for modeling.

Bicubic patches on cones and cylinders. A cone with vertex \mathbf{v} can be written as $\mathbf{x}(u, v) = \mathbf{v} + f(u, v)\mathbf{c}(u)$. To get a bicubic parameterization, we can use a cubic curve $\mathbf{c}(u)$ and a cubic polynomial $f(u, v) = g(v)$ or a quadratic curve (parabola) $\mathbf{c}(u)$ and a function $f(u, v)$ of bi-degree $(1, 3)$. In the former case, the cone is in general a cubic surface, while in the latter case one parameterizes quadratic cones.

A cylinder $\mathbf{x}(u, v) = \mathbf{a}(u) + f(u, v)\mathbf{r}$, with a ruling direction \mathbf{r} , has a bicubic representation when $\mathbf{a}(u)$ is at most cubic and f any bicubic function.

Developable bicubic patches with a planar Gauss image. This class of surfaces includes all bicubic cylinders. Among the cones, only rotational cones are possible. We can generate them from the special cone $x^2 + y^2 = z^2$, and then apply uniform scaling in z -direction and a rigid body motion. The special cone is parameterized by a Pythagorean triple of bicubic functions $x(u, v), y(u, v), z(u, v)$ of the form

$$x(u, v) = 2abw, \quad y(u, v) = (a^2 - b^2)w, \quad z(u, v) = (a^2 + b^2)w,$$

where $a(u, v)$, $b(u, v)$, $w(u, v)$ are bilinear functions. Bicubic tangent surfaces with a planar Gauss image have a regression curve $\mathbf{c}(u)$ of constant slope. It follows from our considerations above that the tangent surface of a polynomial curve $\mathbf{c}(u)$ of constant slope and degree ≤ 4 is such a surface. These curves $\mathbf{c}(u)$ are exactly the *spatial Pythagorean hodograph curves* of degree ≤ 4 . For their generation and degrees of freedom, we point to the monograph by R. Farouki [32, Chapter 21].

We have already mentioned rotational cones and note that rotational cylinders do not possess an exact bicubic parameterization. This is due to the fact that a rotational cylinder cannot carry a polynomial curve transversal to the rulings as it would project onto a circle. While a circle does not have an exact polynomial parameterization, it is possible to achieve good approximations with cubics (see [33] and the references therein). This is sufficient for our purposes.

Developable B-spline surfaces. If two algebraic developable surface patches meet with C^1 continuity at a common curve (different from a ruling), their set of tangent planes agrees there. Due to the algebraic nature, agreement of the set of tangent planes along a curve segment is sufficient for the agreement of the set of tangent planes everywhere and for agreement of the two algebraic surfaces. Therefore, any developable B-spline surface with C^1 continuity represents a single polynomial developable surface, unless the patches are joined along rulings. This latter case is used in [7]. The former case is useful to represent appropriate trimmed patches on polynomial developable surfaces, but not for increasing the flexibility in modeling the surfaces themselves.

A regular bicubic surface \mathbf{S} parameterized by parameters u, v is developable when the Gaussian curvature vanishes at every point $(u, v) \in D$ of the surface. Based on this definition of developable surfaces, we can compute the algebraic complexity of the developability property for \mathbf{S} . Since the Gaussian curvature is the ratio of the determinants of the second and first fundamental forms, it is sufficient for the following equation to hold

$$\det(\mathbf{II}) = 0 \Leftrightarrow [\mathbf{S}_{uu}, \mathbf{S}_u, \mathbf{S}_v][\mathbf{S}_{vv}, \mathbf{S}_u, \mathbf{S}_v] - [\mathbf{S}_{uv}, \mathbf{S}_u, \mathbf{S}_v]^2 = 0, \quad \forall (u, v) \in D$$

where $[\mathbf{a}, \mathbf{b}, \mathbf{c}]$ denotes the triple product of vectors $\mathbf{a}, \mathbf{b}, \mathbf{c} \in \mathbb{R}^3$. Expanding and grouping with respect to monomials in parameters u, v we get a polynomial $f \in \mathbb{R}[x_{00}, y_{00}, z_{00}, \dots, x_{33}, y_{33}, z_{33}][u, v]$, where $(x_{ij}, y_{ij}, z_{ij}) \in \mathbb{R}^3$, are the coordinates of control point $\mathbf{P}_{i,j}$ of surface \mathbf{S} . Following this grouping, we count that polynomial f has 191 coefficients $g_k \in \mathbb{R}[x_{00}, y_{00}, z_{00}, \dots, x_{33}, y_{33}, z_{33}]$, where $k = 1, \dots, 191$.

The requirement that polynomial f vanishes for all values $(u, v) \in D$ is satisfied if f is identically the zero polynomial, or equivalently all coefficient polynomials g_k vanish. This means that, if we need to guarantee these conditions precisely by evaluating f at different points on the surface, we would require a minimum of 191 points in a general position, namely points that would generate linearly independent combinations of g_k . In practice, since $\deg_u(f) = \deg_v(f) = 13$ we would define a 14×14 regular grid over D to acquire 196 evaluation points.

Alternatively, we can examine the algebraic variety $V(I)$ of the ideal $I = \langle g_1, \dots, g_{191} \rangle$ generated by the coefficient polynomials g_k . Again, these are 191 homogeneous polynomials in 48 variables with $\deg(g_k) = 6$. Computing a reduced Gröbner basis in an attempt to work with a minimal number of generators $h_m \in \mathbb{R}[x_{00}, y_{00}, z_{00}, \dots, x_{33}, y_{33}, z_{33}]$, with $m \leq 191$, for the ideal I is computationally expensive, and is expected to produce generators that have increasingly higher degrees [34].

These observations only demonstrate that if we wish to increase interactivity in the design process with developable surfaces, we need to avoid the computational complexity of exact satisfiability and instead sufficiently approximate the developability property in an efficient way.

3. Increasing developability

Motivated by Theorem 2.2, we can try to increase the developability of a surface S by ensuring that the Gauss images of well chosen regions on S are nearly planar. Using this basic idea, we now discuss the details of an optimization algorithm which iteratively deforms a bicubic B-spline surface towards a nearly developable one.

3.1. Optimization setup

Surface. Let us consider a bicubic B-spline surface $\mathbf{S} : \mathbb{R}^2 \rightarrow \mathbb{R}^3$,

$$\mathbf{S}(u, v) = \sum_{i=0}^n \sum_{j=0}^m B_{i,3}(u) B_{j,3}(v) \mathbf{P}_{i,j}, \quad (4)$$

where $u, v \in [0, 1]$ and $B_{i,3}(u), B_{j,3}(v)$ are cubic B-spline basis functions defined on uniform knot sequences in both directions. $\{\mathbf{P}_{i,j}\} \in \mathbb{R}^3$ are the control points of the surface \mathbf{S} , where $0 \leq i \leq n$, $0 \leq j \leq m$ and $n, m \geq 3$. For more information on B-spline surfaces and NURBS surfaces in general, we direct the reader to [35, Section 4.4].

Surface \mathbf{S} serves as the central object of study in this work. A generic surface of the above form is non-developable and we aim to increase its developability by modifying the coordinates of its control points in a "minimal" way that will be defined in the following sections.

We point out that surface \mathbf{S} could be defined as any NURBS surface as long as the weights of the control points and the knot vectors are fixed and are not considered variables in the optimization process. This simplifies and accelerates the optimization procedure while not sacrificing the quality of our results in the sense that B-spline surfaces are adequate approximations of more general NURBS surfaces. For readability, we define \mathbf{S} as an elementary B-spline surface while keeping in mind that the following applies to more general surfaces.

Sampling the surface. We begin by sampling \mathbf{S} , the surface that is to be optimized, at a set of evaluation points $\{\mathbf{p}_k\} \subset \mathbb{R}^3$, which we will call *sample points*.

The approach we took for the sampling was to uniformly sample the parameter space, motivated by the fact that convoluted areas on the surface \mathbf{S} , i.e. areas where the control points are concentrated and finer features emerge, would be represented by more evaluation points inherently. We set the number of sample points L_u, L_v along the u, v directions respectively and get a gridded pattern of points $(u, v) \in [0, \frac{1}{L_u+1}, \dots, 1] \times [0, \frac{1}{L_v+1}, \dots, 1]$ on the parameter space, which in turn results in the set of required sample points $\{\mathbf{p}_k\}$ on the surface \mathbf{S} .

The evaluation of points \mathbf{p}_k is given by formula 4, which is linear in the coordinates of the control points with constant coefficients. In practice, these coefficients are precomputed per point and stored. Whenever the control points are updated by the optimization process or user input, we re-evaluate the position of the sample points using the stored coefficients.

Grouping into patches. Next, we consider overlapping neighborhoods on the surface, that we will call *patches*, and that are represented as sets of sample points U_j . We construct the patches in such a way that neighboring patches will have non-empty intersections, i.e. there exists at least one sample point that belongs to both patches. The importance of this property will become clear in a later section.

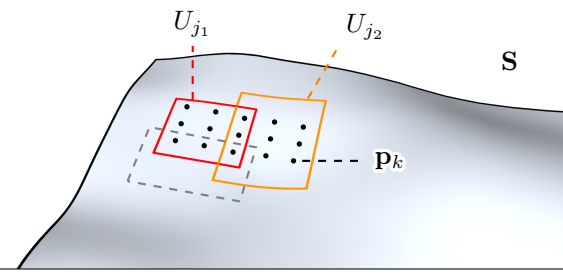


Figure 3: Surface \mathbf{S} is sampled at various evaluation points \mathbf{p}_k . The sample points are then grouped to overlapping groups. An example of such a grouping are groups U_{j_1} and U_{j_2} .

By uniformly sampling the parameter space we also simplify the process of grouping the sample points. The patches on the surface, as already mentioned, are represented by sets of sample points. By using the grid of points on the parameter space we can determine the patches just by setting the number of sample points in each of the u, v directions that a patch will contain and the number of sample points that will belong in the overlap region for each of the u, v directions. Figure 3 focuses on two such patches as an example of a simple grouping.

Normal computation. We associate each sample point \mathbf{p}_k with the unit normal \mathbf{n}_k of the surface at that point. The unit normals define the *Gauss map* σ of the surface. We compute the unit normal \mathbf{n}_k of the surface point \mathbf{p}_k as

$$\mathbf{n}_k := \sigma(\mathbf{p}_k) = \frac{\mathbf{S}_u \times \mathbf{S}_v}{\|\mathbf{S}_u \times \mathbf{S}_v\|},$$

where \mathbf{S}_u , \mathbf{S}_v are the partial derivatives of \mathbf{S} with respect to u and v . Note that \mathbf{S}_u and \mathbf{S}_v ,

$$\mathbf{S}_u(u, v) = \sum_{i=0}^n \sum_{j=0}^m B_{i,3}^{(1)}(u) B_{j,3}(v) \mathbf{P}_{i,j}, \quad \mathbf{S}_v(u, v) = \sum_{i=0}^n \sum_{j=0}^m B_{i,3}(u) B_{j,3}^{(1)}(v) \mathbf{P}_{i,j},$$

are linear combinations of the control points with coefficients which we precompute and store to accelerate future computations [35, Section 1.5].

Gauss map of a patch. For every patch U_j , we denote by N_j the Gauss image of U_j , i.e. the set of unit normals \mathbf{n}_k corresponding to the sample points $\mathbf{p}_k \in U_j$,

$$N_j = \sigma(U_j) = \sigma(\{\mathbf{p}_k\}) = \{\mathbf{n}_k\}.$$

We associate each patch U_j with a plane $H_j \subset \mathbb{R}^3$ with equation $\mathbf{v}_j \cdot \mathbf{x} + d_j = 0$. Here, \mathbf{v}_j is a unit normal vector of H_j and d_j is the distance of H_j from the origin. H_j serves as the target plane for N_j . By optimization, we will enforce all normal vectors in N_j to lie on H_j and thus aim at a planar Gauss image of patch U_j .

3.2. Initialization

The variables of the optimization are the coordinates of the control points $\mathbf{P}_{i,j}$ and the cutting planes H_j that define the Gauss image circles per patch U_j . In this section, we describe the initialization step of the optimization process.

Control points. We assume that we always have an initial state for the surface that is either user defined or is provided by other means. We initialize the control point coordinates with the values from this initial configuration. Those in turn will be used to initialize H_j for every patch.

Cutting planes. We want to optimize for planarity of the Gauss image N_j of each patch U_j and thus associate with each patch U_j a target plane H_j for N_j . Initializing the target plane H_j for each patch with the best fitting plane to points $\mathbf{n}_k \in S^2$ works in the case that U_j is a developable patch. However, this method does not produce the desired results if the patch is non-developable, as seen in Figure 4. To overcome this, we use the following approach.

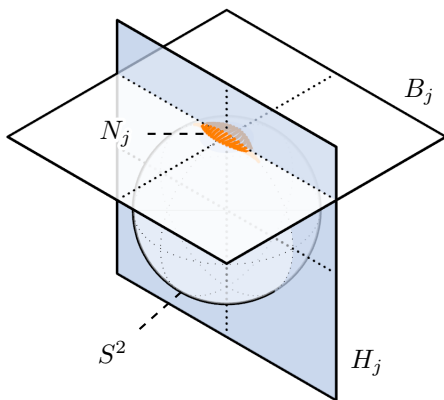


Figure 4: Consider the Gauss image N_j of a group U_j . Plane B_j is the best fitting plane to N_j , in the sense that it minimizes the sum of squared distances of points N_j to the plane, and is considered an undesired initialization. Using B_j as a target plane for the points in N_j will degenerate the Gauss image to a single point, meaning patch U_j will be flat. Alternatively, plane H_j is the resulting plane from optimization problem 1 and captures the overall main principal direction of patch U_j . Plane H_j is a better initial target plane, since it will not necessarily lead to a 0-dimensional Gauss image.

Consider the main principal direction $\mathbf{q}_k \in \mathbb{R}^3$ of surface \mathbf{S} at point \mathbf{p}_k , i.e. the principal direction corresponding to the principal curvature with the maximum absolute value, that is $\max\{|\kappa_1(\mathbf{p}_k)|, |\kappa_2(\mathbf{p}_k)|\}$ where $\kappa_i : \mathbf{S} \rightarrow \mathbb{R}$, $i = 1, 2$, are the principal curvatures of a point on \mathbf{S} . The *principal curvatures* and *principal directions* of a surface at a point on the surface are the eigenvalues and corresponding eigenvectors of the *shape operator* $-d_v \mathbf{N} = -\mathbf{I}^{-1} \mathbf{II}$, where \mathbf{I} , \mathbf{II} are the *first* and *second fundamental forms* of the surface. We denote by Q_j the set of main principal directions \mathbf{q}_k corresponding to the points $\mathbf{p}_k \in U_j$.

We initialize H_j as the plane passing through the barycenter of N_j with unit normal in the direction of the vector which is "as orthogonal as possible" to the set Q_j of main principal directions. Intuitively, we wish the initial cutting plane to intersect the sphere at a circle whose tangent at every point $\mathbf{c} \in S^2 \cap H_j$ is "as parallel as possible" to the main principal directions of the sample points corresponding to the unit normals around \mathbf{c} .

In this way, the cutting plane serves as a generalized main principal plane, or a plane containing the main principal directions of every sample point in the patch. For a patch that is non-developable, we wish to initialize this main principal plane by using the main principal directions of the sample points weighted by a measure of confidence. A low weight indicates the difficulty in distinguishing between the two principal curvatures. Specifically, we introduce weight $w_k \in [0, 1]$ corresponding to each sample point \mathbf{p}_k as

$$w_k = 1 - \frac{\min\{|\kappa_i(\mathbf{p}_k)|\}}{\max\{|\kappa_i(\mathbf{p}_k)|\}}, \quad i = 1, 2 \quad (5)$$

Now, for each patch U_j we need to solve the following optimization problem.

Optimization problem 1 Plane initialization

$$\begin{aligned} & \text{minimize}_{\mathbf{q}_k \in Q_j} \quad \sum_{\mathbf{q}_k \in Q_j} w_k (\mathbf{v}_j \cdot \mathbf{q}_k)^2 \\ & \text{subject to} \quad \mathbf{v}_j^2 = 1 \end{aligned}$$

Optimization problem 1 is a special case of minimizing a quadratic form under a quadratic regularization constraint. Bringing the objective function into the form $\mathbf{v}_j^\top \mathbf{Q} \mathbf{v}_j$, the minimizer \mathbf{v}_j^* is the normalized eigenvector corresponding to the smallest eigenvalue of \mathbf{Q} . Then, plane H_j is given by $\mathbf{v}_j^* \cdot \mathbf{x} + d_j = 0$, with

$$d_j = -\mathbf{v}_j^* \cdot \frac{1}{|N_j|} \sum_{\mathbf{n}_k \in N_j} \mathbf{n}_k,$$

where $|N_j|$ is the cardinality of N_j .

3.3. Problem formulation

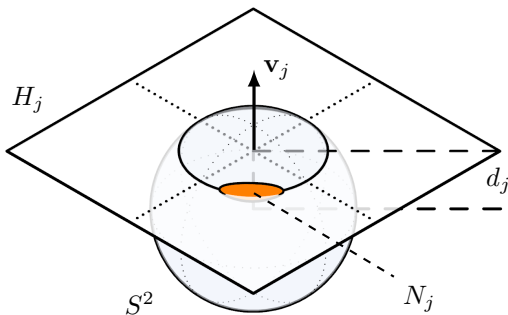


Figure 5: The Gauss image N_j of a single non-developable patch U_j is a 2-dimensional subset of S^2 . The cutting plane H_j serves as the target plane for the normals $\mathbf{n}_k \in N_j$.

Developability energy. We are now ready to formulate the desired property of each patch to have a planar Gauss image by introducing an appropriate energy term E_d . This energy term measures per patch the total sum of distances of the normals $\mathbf{n}_k \in S^2$ to the target patch plane, that is the quantity

$$\sum_j \sum_{\mathbf{n}_k \in N_j} (\mathbf{n}_k \cdot \mathbf{v}_j + d_j)^2, \quad (6)$$

where j is the indexing of the patches and \mathbf{v}_j , d_j are unit normal and distance from the origin of target plane H_j for patch U_j . To avoid trivial solutions, we introduce the following unit length constraint on the plane normals \mathbf{v}_j in the form of an additional energy term,

$$\sum_j (\mathbf{v}_j^2 - 1)^2.$$

Additionally, the surface normals \mathbf{n}_k are computed as

$$\mathbf{n}_k^{(m)} = \frac{\mathbf{S}_u^{(m)} \times \mathbf{S}_v^{(m)}}{\|\mathbf{S}_u^{(m-1)} \times \mathbf{S}_v^{(m-1)}\|},$$

where $a^{(m)}$ denotes the value of variable a at iteration step m in our iterative optimization process. We use the constant norm $\|\mathbf{S}_u^{(m-1)} \times \mathbf{S}_v^{(m-1)}\|$ from the previous iteration when normalizing the current vector $\mathbf{S}_u^{(m)} \times \mathbf{S}_v^{(m)}$ for the computation of the surface normal \mathbf{n}_k . This is standard practice to ensure that the objective function is polynomial.

All the above lead to an energy term of the form

$$E_d = \sum_j \sum_{\mathbf{n}_k \in N_j} (\mathbf{n}_k \cdot \mathbf{v}_j + d_j)^2 + \lambda_1 \sum_j (\mathbf{v}_j^2 - 1)^2, \quad (7)$$

where λ_1 is an appropriate weight for the unit length constraint.

The importance of having patches that are overlapping, or equivalently neighboring patches containing common sample points, becomes evident at this point. Each patch is optimized to have a Gauss image which is a subset of a spherical curve. This can have a competitive effect between patches that are adjacent due to diverging target planes, and cause slow convergence. By having the patches share sample points, we introduce a diffusion factor to the optimization that ensures smoothness of the resulting Gauss image curve.

Soft constraints. We also introduce a set of additional energy terms to the main problem that constrain the output surface and aim to avoid degeneracies, produce more aesthetically pleasing results and give control to the user over the proximity of the resulting surface to a reference surface.

The energy term E_c denotes a measure of the closeness of the resulting surface \mathbf{S} to a reference surface \mathbf{S}_{ref} , which can be either an arbitrary surface or the initial configuration of the design surface. The implementation we follow for the closeness energy term is based on the *tangential distance minimization* (TDM) [36, 37]. The energy term is defined as the sum of squared distances of sample points to the tangent planes at their closest points on the reference surface. We use the already sampled points $\mathbf{p}_k \in \mathbf{S}$ and a set of sample points X from the reference surface \mathbf{S}_{ref} . If the reference surface is the initial surface then $X = \{\mathbf{p}_k\}$; otherwise, X is an independent sampling. Then E_c is defined as

$$E_c = \sum_k [(\mathbf{p}_k - \mathbf{x}_k) \cdot \mathbf{N}(\mathbf{x}_k)]^2, \quad (8)$$

where \mathbf{x}_k is the closest point to \mathbf{p}_k from the set of points X in the Euclidean metric, and $\mathbf{N}(\mathbf{x}_k)$ is the unit normal of \mathbf{S}_{ref} at point \mathbf{x}_k . At each iteration the closest point is updated. We utilize FLANN for the closest point query and refer to [38] for the computational complexity.

A final fairness energy term $E_f = w_{f_1} E_{f_1} + w_{f_2} E_{f_2}$ is introduced to the objective function that avoids degeneracies in the resulting surface and is widely used in mesh optimization problems for the smoothing effect it provides. Specifically, we denote by E_{f_1} the sum of squared norms of the first order differences of the control points in both grid directions, and by E_{f_2} the second order equivalent, namely

$$\begin{aligned} E_{f_1} &= \sum_{i,j} (\|\mathbf{P}_{i+1,j} - \mathbf{P}_{i,j}\|^2 + \|\mathbf{P}_{i,j+1} - \mathbf{P}_{i,j}\|^2), \\ E_{f_2} &= \sum_{i,j} (\|\mathbf{P}_{i+1,j} - 2\mathbf{P}_{i,j} + \mathbf{P}_{i-1,j}\|^2 + \|\mathbf{P}_{i,j+1} - 2\mathbf{P}_{i,j} + \mathbf{P}_{i,j-1}\|^2). \end{aligned}$$

We assign $w_{f_1} = 0$, $w_{f_2} = 1$ in all the following applications unless stated otherwise.

Total energy. All energy terms E_d , E_c , E_f are assigned weights w_d , w_c , w_f and collected in the total energy for developability optimization,

$$E = w_d E_d + w_c E_c + w_f E_f. \quad (9)$$

For details on the choice of weights, we refer to Section 5.

Increasing developability. Now our problem is reduced to the minimization of E .

Optimization problem 2 Increasing developability

$$\text{minimize} \quad E = w_d E_d + w_c E_c + w_f E_f$$

The variables of E are the control points $\{\mathbf{P}_{i,j}\}$ of \mathbf{S} and the patch planes H_j , defined by \mathbf{v}_j and d_j . The optimization problem 2 is an unconstrained nonlinear least-squares problem. Any algorithm for nonlinear least-squares problem can be applied in our case. We follow the standard *Gauss-Newton method* in our implementation and experiments [39, Section 10.3].

4. Panelization

Motivated by applications in architecture, we consider the problem of approximating a given arbitrary surface by a C^0 continuous surface which consists of developable patches. As we optimize for developability with help of a planar Gauss image, the resulting surface patches include as important special cases rotational cylinders and rotational cones. We will particularly focus on the constraints which ensure that we obtain these special types of panels. Especially when working with glass, these rotational panels are preferred because there are special machines for their production. Figure 6 shows a recent example of an architectural freeform facade which has been constructed with mainly cylindrical glass panels to reduce manufacturing cost.



Figure 6: Side detail of *Nur Alem*, the main pavilion of the Astana EXPO 2017 Exhibition in Astana, Kazakhstan. Mostly cylindrical panels were used to rationalize the curved transparent freeform façade (different from the sphere).

In this section, we will go through the differences between the central method that was presented in the previous sections and the variation for this new problem while introducing any new concepts that will be of use.

Surface. The main object of study in this section will be a surface \mathbf{S} consisting of a grid of subsurfaces $\mathbf{S}^{(r)}$, with C^0 continuity at the inner boundaries. Specifically, \mathbf{S} is a composite surface

$$\mathbf{S} = \bigcup_r \mathbf{S}^{(r)},$$

where r indexes the set of subsurfaces. Each $\mathbf{S}^{(r)}$ is a bicubic Bézier surface of the form

$$\mathbf{S}^{(r)}(u, v) = \sum_{i=0}^3 \sum_{j=0}^3 B_{i,3}(u) B_{j,3}(v) \mathbf{P}_{i,j}^{(r)} \quad (10)$$

and will be referred to as a *panel* in the following. This configuration represents the paneling of a freeform surface. The C^0 continuity of neighboring panels is achieved by having common control points at the corresponding edges and models the connectivity and continuity found between

distinct panels of a panelized surface. This allows for panelizations that are not in a grid configuration and can easily generalize to more complex surfaces of arbitrary topology just by appropriately "gluing" panels at their edges.

Sampling and grouping. We sample surface \mathbf{S} at a collection of sample points $\{\mathbf{p}_k\}$ and group them to groups U_r , each corresponding to a single panel. The same follows for the corresponding surface normals N_r and the associated panel planes H_r .

We can therefore define the developability energy term per panel as

$$E_d^{(r)} = \sum_{\mathbf{n}_k \in N_r} (\mathbf{n}_k \cdot \mathbf{v}_r + d_r)^2 + \lambda_1(\mathbf{v}_r^2 - 1)^2, \quad (11)$$

where λ_1 is an appropriate weight, and the developability energy term of surface \mathbf{S} as

$$E_d = \sum_r E_d^{(r)}. \quad (12)$$

This modified grouping of the sample points $\{\mathbf{p}_k\}$ allows for the individual optimization of each panel, which will be studied in more detail in a following section.

Rotational panels. By introducing the additional constraint that the panel should be a rotational surface, we are optimizing for the panels to be either rotational cones or rotational cylinders. Rotational surfaces have the property that the surface normal lines are coplanar with the axis of rotation. Let L_1, L_2 be two lines in \mathbb{R}^3 with Plücker coordinates $(\mathbf{a}, \bar{\mathbf{a}}), (\mathbf{b}, \bar{\mathbf{b}}) \in \mathbb{R}^6$ respectively. The two lines are coplanar if their Plücker coordinates satisfy the condition

$$\mathbf{a} \cdot \bar{\mathbf{b}} + \bar{\mathbf{a}} \cdot \mathbf{b} = 0. \quad (13)$$

Recall that the Plücker coordinates $(\mathbf{a}, \bar{\mathbf{a}}) \in \mathbb{R}^6$ of a line $L \subset \mathbb{R}^3$ are given by the direction vector $\mathbf{a} \in \mathbb{R}^3$ and the moment vector $\bar{\mathbf{a}} = \mathbf{p} \times \mathbf{a} \in \mathbb{R}^3$, where $\mathbf{p} \in \mathbb{R}^3$ is a point on L . Obviously, these coordinates are not independent, but satisfy the Plücker condition $\mathbf{a} \cdot \bar{\mathbf{a}} = 0$. For more information on line geometry and relevant applications, we refer to the literature [6, Section 2.1].

Consider now the Plücker coordinates $(\mathbf{n}_k, \bar{\mathbf{n}}_k) \in \mathbb{R}^6$ of the normal lines at the sample points of a panel U_r and of the unknown axis of rotation $(\mathbf{a}_r, \bar{\mathbf{a}}_r) \in \mathbb{R}^6$. The desired property that the panel is a rotational surface can be expressed as $\mathbf{a}_r \cdot \bar{\mathbf{n}}_k + \mathbf{n}_k \cdot \bar{\mathbf{a}}_r = 0 \forall \mathbf{n}_k \in N_r$. Thus, the problem of optimizing for rotational surface panels can be formulated as minimizing the energy

$$\sum_r \sum_{\mathbf{n}_k \in N_r} (\mathbf{a}_r \cdot \bar{\mathbf{n}}_k + \mathbf{n}_k \cdot \bar{\mathbf{a}}_r)^2, \quad (14)$$

under the constraint that $(\mathbf{a}_r, \bar{\mathbf{a}}_r)$ describe a line, i.e., satisfy the Plücker condition $\mathbf{a}_r \cdot \bar{\mathbf{a}}_r = 0$, and the unit length constraint $\mathbf{a}_r^2 = 1$ on the axis direction \mathbf{a}_r .

At this point, we focus on the fact that for a rotational panel $S^{(r)}$ with planar Gauss image, the normal \mathbf{v}_r of the plane H_r containing the Gauss image and the direction of the rotation axis \mathbf{a}_r coincide. Using this fact, we denote the Plücker coordinates of the rotation axis by $(\mathbf{v}_r, \bar{\mathbf{v}}_r)$.

By making this adaptation, we have covered the unit length constraint on the rotation axis direction by the corresponding constraint on the target plane normal in (11). The Plücker condition is added as an additional energy term with an appropriate weight λ_2 . Considering all the above, the resulting rotationality energy term E_r is of the form

$$E_r = \sum_r \sum_{\mathbf{n}_k \in N_r} (\mathbf{v}_r \cdot \bar{\mathbf{n}}_k + \mathbf{n}_k \cdot \bar{\mathbf{v}}_r)^2 + \lambda_2 \sum_r (\mathbf{v}_r \cdot \bar{\mathbf{v}}_r)^2. \quad (15)$$

While the Plücker coordinates of the normal lines are initialized in the optimization problem with their current values in the configuration of surface \mathbf{S} , the axis of rotation $(\mathbf{v}_r, \bar{\mathbf{v}}_r)$ of every panel U_r remains unknown at this point or, assuming the panels are in generic configuration, does not exist at all. An appropriate initialization for the Plücker coordinates of the axis of rotation of each panel is given by methods used in kinematic surface reconstruction applications, where the problem of fitting a velocity field to a set of surface normals is studied [40, 41]. It follows the same thought process as the main idea behind the energy term (14). In fact, it is exactly the same energy that we aim to minimize but applied to each of the panels separately while considering

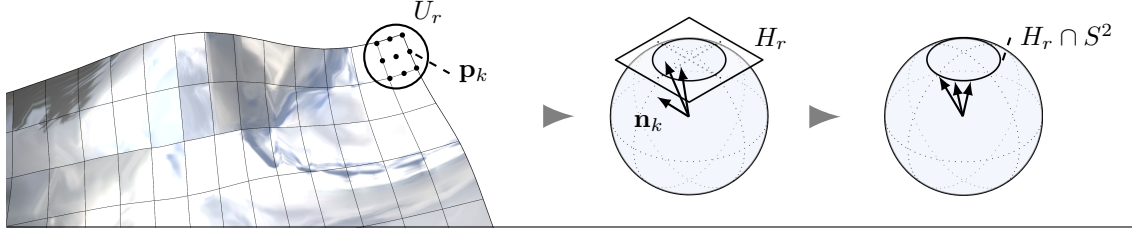


Figure 7: We focus on a single panel $\mathbf{S}^{(r)}$ of a panelized surface \mathbf{S} . We are optimizing for the endpoints of normals \mathbf{n}_k corresponding to the sample points $\mathbf{p}_k \in U_r$ of panel $\mathbf{S}^{(r)}$ to lie on the same plane H_r .

the affine normal lines fixed. The resulting axis is the best fitting one in the least-squares sense. Formulating the above as an optimization problem leads us to the minimization of

$$\sum_{\mathbf{n}_k \in N_r} (\mathbf{v}_r \cdot \bar{\mathbf{n}}_k + \bar{\mathbf{v}}_r \cdot \mathbf{n}_k)^2. \quad (16)$$

We already have an appropriate initialization for the target plane normal \mathbf{v}_r , described in optimization problem 1. Thus, the objective function (16) is a quadratic function of the moment vector $\bar{\mathbf{v}}_r$. The latter is orthogonal to \mathbf{v}_r and therefore can be expressed as

$$\bar{\mathbf{v}}_r = \mu_1 \mathbf{b}_1 + \mu_2 \mathbf{b}_2,$$

where $\mathbf{b}_1, \mathbf{b}_2 \in \mathbb{R}^3$ form a basis of the plane perpendicular to \mathbf{v}_r . Substitution into (16) yields a quadratic function in μ_1, μ_2 and the optimal values of μ_1, μ_2 are the solutions of a linear system.

Surface paneling. Thus, the surface paneling problem is the following variation of the optimization problem 2, and is solved with the same approach.

Optimization problem 3 Surface paneling

$$\text{minimize } E = w_d E_d + w_r E_r + w_c E_c + w_f E_f$$

Individual panel treatment. Until now we have shown how to optimize the paneling of surface \mathbf{S} in a global fashion. Since we defined the energy term $E_d^{(r)}$ per panel, this approach can be customized to consider each panel separately, achieving in the process increased control over the resulting panelization. We use the following obvious fact:

Lemma 4.1. *Let panel $\mathbf{S}^{(r)}$ be a rotational surface and H_r be a plane such that the Gauss image of the panel is entirely contained in plane H_r . Then the panel type is determined by the distance d_r of plane H_r from the origin O . Specifically,*

1. *If $d_r = 1$ then $\mathbf{S}^{(r)}$ is planar.*
2. *If $d_r = 0$ then $\mathbf{S}^{(r)}$ is a cylinder of revolution.*
3. *If $d_r \in (0, 1)$ then $\mathbf{S}^{(r)}$ is a cone of revolution whose rulings form the angle $\arcsin d_r$ with the rotation axis.*

This offers a good way to aim at cylindrical panels or conical panels with prescribed opening angle by prescribing the according values of d_r in the energy term $E_d^{(r)}$ in (11).

It is often the case in industrial applications that individual adjustments need to be made to the panelization for reasons that include aesthetics and the overall cost of the project. The advantages of the individual treatment of the panels become apparent in such cases, and the aforementioned main pavilion of the Astana EXPO 2017, shown in Figure 6, serves as an example. In that project, apart from the cylindrical panels which were the main ingredient of the panelization, double curved panels were also utilized in areas that the use of cylindrical panels would negatively affect the aesthetics of the result. Thus, by integrating a singular panel management strategy to the optimization we have the ability of dealing with isolated problematic areas without sacrificing the quality of the overall panelization.

5. Experiments, results and discussion

Example 5.1. In this example, we consider a mesh \mathcal{M} which originated from scanning a thin deformed leather patch. The deformation was introduced to the material in the form of local stretches along its surface which result in areas of nonzero Gaussian curvature.

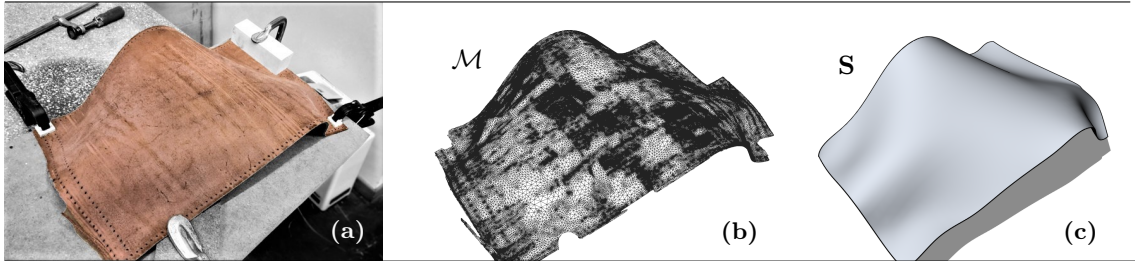


Figure 8: (a) The configuration of the deformed leather patch. (b) Mesh acquired from scanning the leather material. (c) The material's geometry is represented as a B-spline surface.

To apply our algorithm for increasing developability, we first fit the data with a bicubic B-spline surface \mathbf{S} of the form (4) with 7×13 control points. This is done using the TDM optimization framework for surface fitting described in section 3.3. We refer to the initial configuration of surface \mathbf{S} , given by the fitting optimization, as \mathbf{S}_0 . Following the procedure described in section 3.1, we sample the resulting surface \mathbf{S} uniformly along the parameter space at 30×60 evaluation points $\mathbf{p}_{i,j}$, $i \in [1, 30]$, $j \in [1, 60]$. We then group $\mathbf{p}_{i,j}$ in patches $U_{l,m}$, each one containing 5×5 points with an overlap in both directions of 2 points between neighboring patches, i.e. $U_{l,m} = \{\mathbf{p}_{i,j} \mid i \in [3l-2, 3l+2], j \in [3m-2, 3m+2]\}$. This completes the initialization of the optimization algorithm of problem 2.

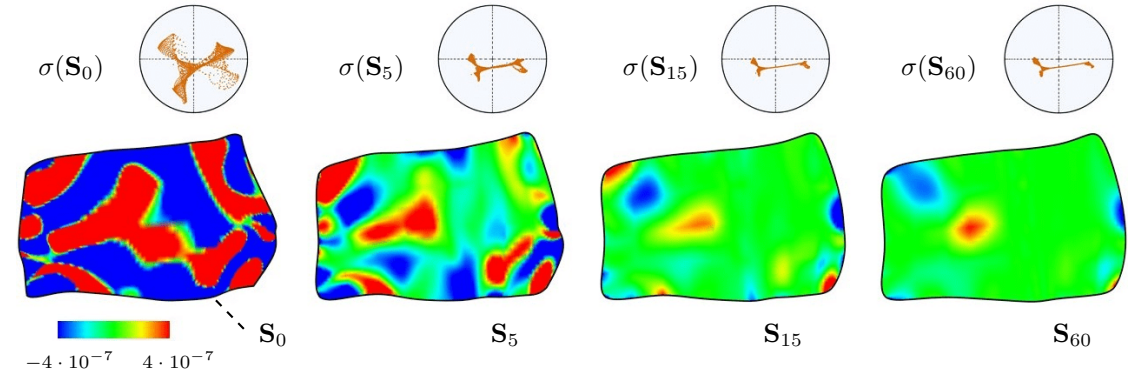


Figure 9: The Gauss map (top) and the Gaussian curvature (bottom) of surface \mathbf{S} for different numbers of iterations, namely at 0, 5, 15 and 60 (\mathbf{S}_t denotes the optimized surface at t iterations). The length of the surface has been scaled to be approximately 1.

We introduce to the optimization process a closeness energy term of the form (8) with relatively small weight to ensure proximity of \mathbf{S} to its original position \mathbf{S}_0 . As described before, this is implemented using the TDM framework. We consider the original surface \mathbf{S}_0 as the reference surface and use the already sampled points $\mathbf{p}_{i,j}$ of surface \mathbf{S} as the evaluation points of the TDM algorithm. In our experiments, we observed that using this competing low-weight term in our main optimization procedure constrains the solution space by avoiding trivial solutions and producing results that are more desirable from the designer's point of view.

Figure 10 reveals the inner workings of the developability algorithm, which clearly produces a "thinner" Gauss image for the resulting surface and also illustrates a comparison between the original surface \mathbf{S}_0 and the resulting surface \mathbf{S} . Figure 9 shows the Gauss map and the Gaussian curvature of the surface for several intermediate iterations of the optimization. The detailed statistics for this example are given in Table 1.

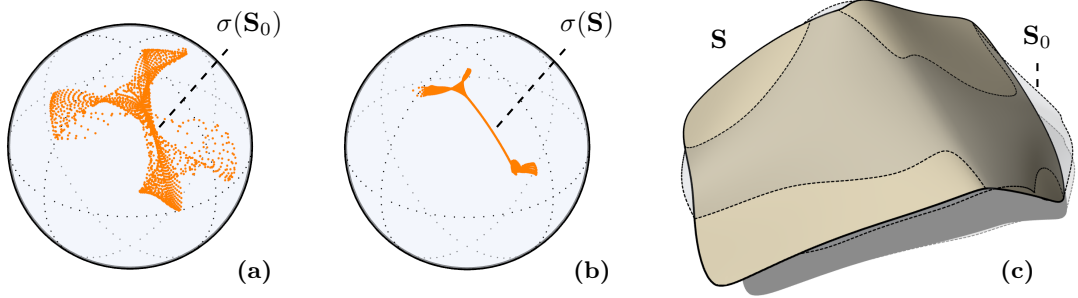


Figure 10: (a) The Gauss image of the initial configuration of B-spline surface S_0 representing the leather material. (b) The Gauss image of the optimized surface S . (c) The optimized B-spline surface S in solid color compared to the transparent initial surface S_0 .

We already discussed in section 2.2 that the straightening of one family of principal curvature lines of S compared to the principal curvature lines of the initial surface S_0 is an alternative indication of the increase in developability. Figure 11 demonstrates the straightening effect in this example. Also illustrated is that the preimage of a small collection of points in one of the "thinner" parts of the Gauss image corresponds to one of the approximate rulings of the surface.

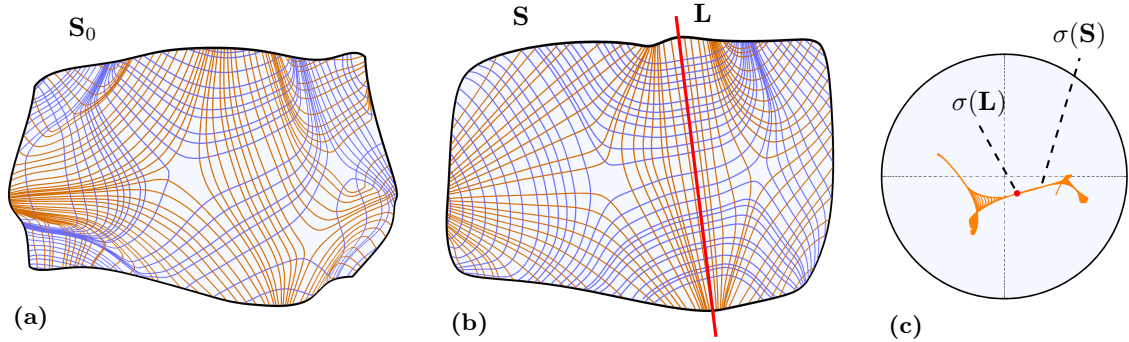


Figure 11: Visualization of the principal curvature lines. (a) The principal curvature lines of the initial surface S_0 . (b) The principal curvature lines of the optimized surface S . Highlighted in red and extended slightly for clarity, one such principal curvature line L , which also approximately corresponds to the preimage of a small collection of points around the "thin" part of $\sigma(S)$. (c) The Gauss image $\sigma(S)$ of the optimized surface S . The Gauss image of L is highlighted in red.

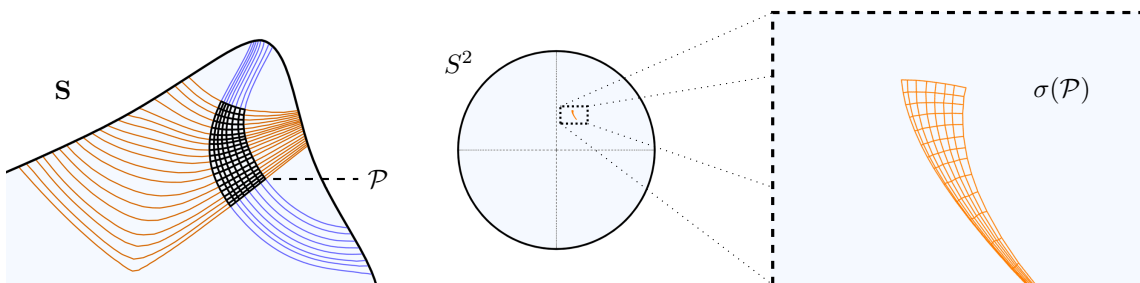


Figure 12: We consider a nearly developable patch of a surface S and the two families of principal curvature lines of S (blue and orange lines) over that patch. These families define a principal net denoted with \mathcal{P} . The Gauss image $\sigma(\mathcal{P})$ of the net is displayed on the right.

ctrl.pts	number of...			weights			final energies			number of iterations	time [sec]		
	patches	variables	eval.pts	w_d	w_c	w_f	E_d	E_c	E_f		T_{total}	T_{solver}	T_{iter}
91	200	1073	1800	100	0.01	0.1	2.54	1.8	0.74	60	121.76	0.13	2.03

Table 1: We present the detailed information for the optimization of the leather surface \mathbf{S} . The number of control points of \mathbf{S} and the number of overlapping patches that cover the surface generate the number of variables (3 per control point and 4 per patch-associated plane). The surface was evaluated at 1800 points and each patch contained 25 points. The weights were chosen to favor the developability property. The initial and intermediate total energies of the problem were $E_0 = 9328.17$, $E_5 = 2103.75$, $E_{15} = 356.702$ while the order of the final total energy $E_{60} = 5.08$ was achieved at iteration 26, where $E_{26} = 5.38$. Also provided, the total time, time used by the Newton solver, and the time per iteration (in seconds), measured on an Intel® Core™ i7-6700HQ processor.

Example 5.2. In this example, we will focus on optimizing two relatively simple non-developable surfaces for planarity of their respective Gauss images. We start with two bicubic Bézier surfaces \mathbf{S}_0^a and \mathbf{S}_0^b , where \mathbf{S}_0^a is of mainly negative Gaussian curvature and \mathbf{S}_0^b of positive Gaussian curvature.

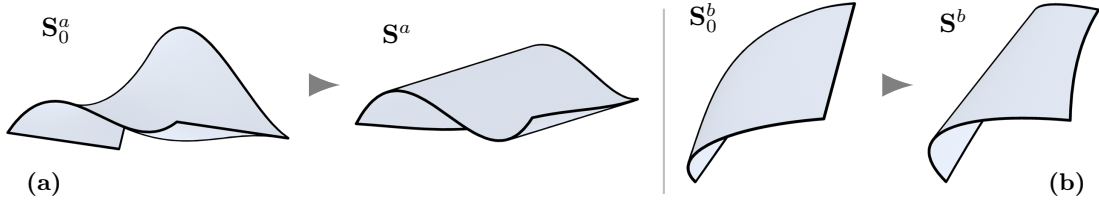


Figure 13: The initial surfaces \mathbf{S}_0^a , \mathbf{S}_0^b and the optimized surfaces \mathbf{S}^a , \mathbf{S}^b are shown from an appropriate angle to better showcase the emergence of rulings in the direction of least absolute principal curvature on each of the surfaces.

We follow optimization problem 3, defined over a single panel, and utilize only the closeness and developability terms. Given that the surfaces have approximately planar Gauss images after the optimization, we also execute the following procedure at a point set U on the surface to extrapolate the approximate rulings that are derived from their planar Gauss images, defined by the target plane H . We do this to present a visual comparison between these induced rulings and the computed rulings on the optimized surface.

Procedure Induced rulings

```

for all  $\mathbf{p} \in U$  do
     $\mathbf{n} \leftarrow \sigma(\mathbf{p})$ 
     $\mathbf{q} \leftarrow \text{closest point of } \mathbf{n} \text{ to target circle } H \cap S^2$ 
     $\mathbf{r}_q^t \leftarrow \text{vector tangent to target circle at } \mathbf{q}$ 
     $\mathbf{r}_q^o \leftarrow \text{vector tangent to } S^2 \text{ at } \mathbf{q} \text{ and orthogonal to } \mathbf{r}_q^t$             $\triangleright \text{induced ruling direction}$ 
     $\text{translate vectors } \mathbf{r}_q^t, \mathbf{r}_q^o \text{ to } \mathbf{p}$ 
end for

```

The vector \mathbf{r}_q^o approximates the direction of the line generator of the surface at point \mathbf{q} . Moreover, for non-inflection rulings and non-planar regions on the optimized surfaces, vectors \mathbf{r}_q^t , \mathbf{r}_q^o correspond to the principal directions of the surface at point \mathbf{q} .

Figure 13 shows the surfaces before and after the optimization, while Figure 14 shows the resulting vectors from the *Induced rulings* procedure.

Fig. No.	number of...				weights		final energies		number of iterations	time [sec]		
	ctrl.pts	panels	variables	eval.pts	w_d	w_c	E_d	E_c		T_{total}	T_{solver}	T_{iter}
13a	16	1	52	169	100	1	0.65	81.28	10	1.9	0.1	0.19
13b	16	1	52	169	100	1	1.45	99.21	10	2.05	0.02	0.2

Table 2: The statistics for the Gauss image planarity optimization of panel surfaces \mathbf{S}_0^a and \mathbf{S}_0^b . The weights were chosen to favor the developability property. Also provided, the total time, time used by the Newton solver, and the time per iteration (in seconds), measured on an Intel® Core™ i7-6700HQ processor.

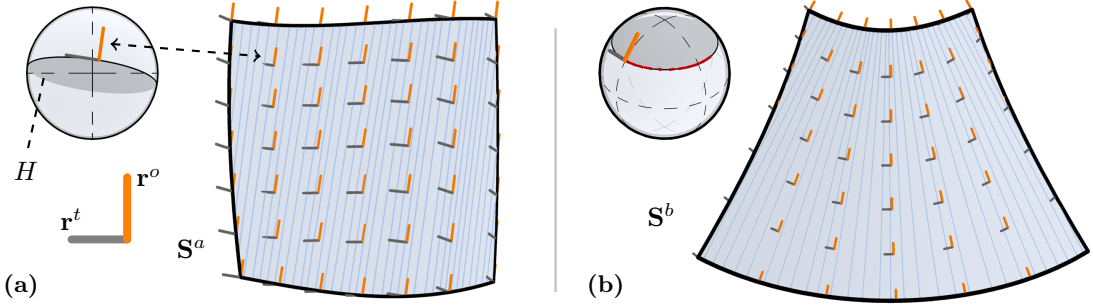


Figure 14: A top-down perspective of the optimized surfaces \mathbf{S}^a , \mathbf{S}^b is shown with the rulings superimposed on the surfaces (darker blue lines) as well as the resulting vectors from the predefined *Induced rulings* procedure. We draw attention to the comparison between the orthogonal vectors \mathbf{r}^o (orange) and the direction of the rulings (vanishing principal curvature direction). Furthermore, vectors \mathbf{r}^t correspond to the directions of nonzero principal direction.

Example 5.3. We provide here an introductory example of paneling a simple double curved surface with a variable number of rotational cylindrical panels.

We consider a surface \mathbf{S}_{ref} which is a subset of the positive-Gaussian-curvature part of a torus. The active surface \mathbf{S} of the optimization consists of a $N \times 1$ grid of bicubic panels. The initial configuration of \mathbf{S} is given by fitting surface \mathbf{S} to \mathbf{S}_{ref} .

We optimize for the panels of \mathbf{S} to be rotational cylinders in the following manner. First of all, we use Lemma 4.1 and assign to each panel an energy term of the form (11) with $d_r = 0$ since we are interested in only cylindrical panels. We then solve optimization problem 3 with equal weights assigned to E_d and E_r , and relatively smaller weights assigned to E_c and E_f .

Figure 15 shows the resulting panelization for different values of N . We wish to direct the reader's focus to the curved boundary lines that follow the reference design; a characteristic not present and inherently not possible without trimming in previous approaches that utilized strips linear in one direction.

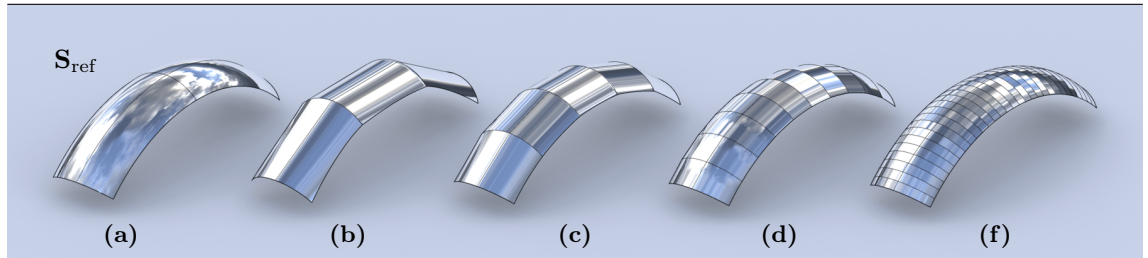


Figure 15: Paneling part of a torus with a different number of cylindrical panels. Both the cutting planes U_r per panel $\mathbf{S}^{(r)}$ and the inner boundary curves follow the direction of the smaller radius circles that define the torus.

Fig. No.	number of...			weights				final energies			number of iterations	time [sec]		
	ctrl.pts	panels	variables	w_d	w_r	w_c	w_f	E_{d+r}^\dagger	E_c	E_f		T_{total}	T_{solver}	T_{iter}
15b	40	3	132	10^2	1	1	0.1	0.043	9.97	5.05	5	1.12	0.02	0.22
15c	64	5	212	10^2	1	1	0.1	0.004	2.09	5.01	5	2.05	0.03	0.4
15d	124	10	412	10^3	10	1	0.1	0.003	0.26	7.11	5	2.99	0.05	0.6
15e	364	30	1212	10^3	10	1	0.1	0.0002	0.05	18.68	5	8.11	0.17	1.62

$$^\dagger E_{d+r} = E_d + E_r$$

Table 3: The statistics for the paneling of the torus subsurface \mathbf{S}_{ref} for different numbers of panels. Each panel was sampled uniformly at 4×4 points for the developability term and at 10×10 points for the closeness term. The weights were chosen to favor the developability property. Also provided, the total time, time used by the Newton solver, and the time per iteration (in seconds), measured on an Intel® Core™ i7-6700HQ processor.

Example 5.4. We extend the previous example of optimizing a simple row of panels to be of cylindrical type to the task of optimizing a grid of panels to be of any developable type we have previously addressed for panels.

Motivated by the possible architectural applications of the algorithm presented in this paper, we use as a reference surface an architectural surface recently realized as the roof of the Department of Islamic Art at Musée du Louvre in Paris, France, shown in Figure 16. The underlying surface is a highly non-developable surface with a strong variation in the sign of Gaussian curvature. In this example, we set forth to compute an alternative realization of the same surface by using rotational conical and rotational cylindrical panels.



Figure 16: Detail from the *Cour Visconti* roof of the Department of Islamic Art at Musée du Louvre in Paris, France.

The user input in this case is the freeform reference surface \mathbf{S}_{ref} , the desired number of panels in each direction of the grid that will constitute the panelization of the surface and the preferred type of panels, which includes surfaces of constant slope or the more specialized and more widely-used rotational surfaces of constant slope, i.e. rotational conical and rotational cylindrical. The user by adjusting the weights of the different energy terms involved in the corresponding optimization problem 3, has influence over the various desirable aspects of the resulting panelization. In this particular example, we wish to use any of the types introduced before, namely rotational conical, rotational cylindrical and planar panels.

We present in Figure 17 the resulting panelization of the reference surface for different panel grid resolutions. We set weight w_c , corresponding to the closeness of \mathbf{S} to \mathbf{S}_{ref} , relatively high to reinforce the resulting surface to not deviate significantly from the reference surface and closely follow the chosen design. The smoothness of the boundary curves is controlled by the fairness energy term weight w_f , which is assigned a small value to ensure more visually pleasing results.

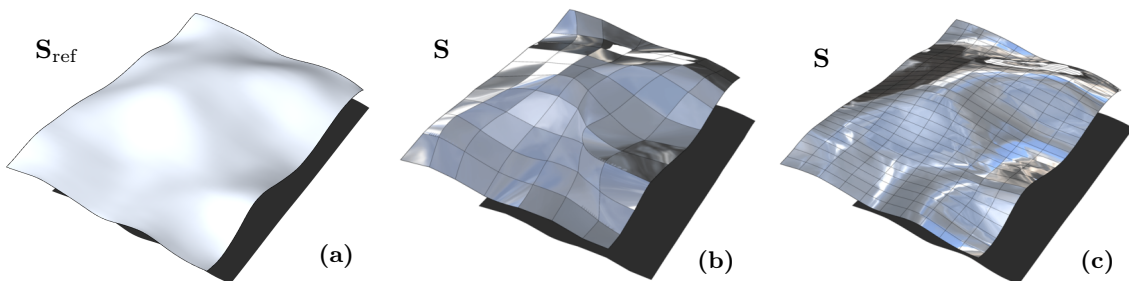


Figure 17: (a) The freeform reference surface to be panelized. (b) A coarse panelization consisting of 70 panels. (c) A denser panelization consisting of 300 panels. Runtime for both the coarse and the finer paneling was several minutes.

The coarse panelization of Figure 17b serves as a nice example of the dynamic panel layout adaptation which aims to approximate the given reference surface while satisfying the developability, rotationality and closeness constraints. On the contrary, by increasing the number of the

panels utilized, we achieve the dense panelization of Figure 17c. As expected the increased number of panels produces an improved result, compared to the coarse equivalent. It not only better approximates the reference surface but also satisfies to a higher degree the additional secondary constraints, yielding a panelization of the reference surface that allows for a more structured arrangement of the panels.

Nevertheless, both results are welcome since each one of them serves as a valid panelization with specialized developables of the same architectural surface. Each one of the two panelizations of this example shown in Figures 17b, 17c manages to be architecturally aesthetically pleasing in its own style, while being realizable only by rotational cylindrical and rotational conical panels; highlighting the freedom of design expression that this method provides.

Short discussion. Appropriate choice of weights leads to high-precision satisfaction of the hard nonlinear constraints. The fairness and closeness terms act as regularizers to the optimization problem, which is formulated through simple polynomial energies. The combination of the soft constraints and fixed points, avoids degenerate results. The complexity of the approach is derived by the degree of the surface to be optimized, the reference surface (number of points of mesh representation) and number of evaluation points. In most applications, our experiments show that the computation time is limited to several seconds to get satisfactory results.

The presented local shaping approach achieves to minimize the predefined energies at every step, and guides iteratively the surface to an expected result. Any unwanted results were limited to surfaces that could not satisfy adequately both the closeness term and the developability term, meaning the result had to deviate considerably from the reference to satisfy the developability constraint.

Limitations. Among the limitations of our research, we first point to the lack of a material-dependent measure for the deviation from developability. The thickness of the Gauss image alone is not sufficient for judging whether a panel, fabricated from hardly stretchable material, can be easily bent into the computed shape. Moreover, our current implementation for paneling is limited to a grid type arrangement of panels and could benefit from additional improvements to the optimizer.

Conclusion. We have introduced a methodology for increasing the developability of surfaces through an optimization algorithm which aims at a thin Gauss image. Our implementation uses B-spline surfaces, but an analogous approach could be formulated for other surface representations as well. Moreover, we have presented a novel paneling algorithm which—in contract to prior work [26]—optimizes both for the panels and the curve network of panel boundaries, under the constraint that panels are developable with a planar Gauss image and/or rotational.

Future work. A promising and important direction for future work is to incorporate a specific material behavior. For example, it would be nice to come up with an efficient algorithm that automatically enforces the design of only those surfaces which can easily be produced from a given material. In particular, materials which bend much more easily than they stretch are of high interest. This leads into the geometrically largely unexplored area of nearly developable surfaces. The paneling algorithm would greatly benefit from an extension to more general panel arrangements, maybe incorporating user interaction supported by automatic suggestions of the system.

6. Acknowledgements

We would like to thank Heinz Schmiedhofer for providing the scan and picture of the leather surface example in Figure 8. This project has received funding from the European Union’s Horizon 2020 research and innovation programme under the Marie Skłodowska-Curie grant agreement No 675789.

References

- [1] J. Lang, O. Röschel, Developable $(1, n)$ -Bézier surfaces, Computer Aided Geometric Design 9 (4) (1992) 291 – 298. [doi:10.1016/0167-8396\(92\)90036-0](https://doi.org/10.1016/0167-8396(92)90036-0).
- [2] G. Aumann, Interpolation with developable Bézier patches, Computer Aided Geometric Design 8 (5) (1991) 409 – 420. [doi:10.1016/0167-8396\(91\)90014-3](https://doi.org/10.1016/0167-8396(91)90014-3).

- [3] G. Aumann, A simple algorithm for designing developable Bézier surfaces, Computer Aided Geometric Design 20 (8-9) (2003) 601–619. [doi:10.1016/j.cagd.2003.07.001](https://doi.org/10.1016/j.cagd.2003.07.001).
- [4] C.-H. Chu, C. Séquin, Developable Bézier patches: properties and design, Computer-Aided Design 34 (7) (2002) 511 – 527. [doi:10.1016/S0010-4485\(01\)00122-1](https://doi.org/10.1016/S0010-4485(01)00122-1).
- [5] C.-H. Chu, J.-T. Chen, Geometric design of uniform developable B-spline surfaces, in: International Design Engineering Technical Conferences and Computers and Information in Engineering Conference, Vol. 1: 30th Design Automation Conference, 2004, pp. 431–436. [doi:10.1115/DETC2004-57257](https://doi.org/10.1115/DETC2004-57257).
- [6] H. Pottmann, J. Wallner, Computational Line Geometry, Springer, 2001. [doi:10.1007/978-3-642-04018-4](https://doi.org/10.1007/978-3-642-04018-4).
- [7] C. Tang, P. Bo, J. Wallner, H. Pottmann, Interactive design of developable surfaces, ACM Transactions on Graphics 35 (2) (2016) 12:1–12:12. [doi:10.1145/2832906](https://doi.org/10.1145/2832906).
- [8] W. Frey, Modeling buckled developable surfaces by triangulation, Computer-Aided Design 36 (4) (2004) 299 – 313. [doi:10.1016/S0010-4485\(03\)00105-2](https://doi.org/10.1016/S0010-4485(03)00105-2).
- [9] J. Mitani, H. Suzuki, Making papercraft toys from meshes using strip approximate unfolding, ACM Transactions on Graphics 23 (3) (2004) 259–263, Proc. SIGGRAPH. [doi:10.1145/1015706.1015711](https://doi.org/10.1145/1015706.1015711).
- [10] K. Rose, A. Sheffer, J. Wither, M.-P. Cani, B. Thibert, Developable surfaces from arbitrary sketched boundaries, in: Proceedings of the Fifth Eurographics Symposium on Geometry Processing, SGP '07, Eurographics Association, 2007, pp. 163–172.
- [11] C. Wang, K. Tang, Achieving developability of a polygonal surface by minimum deformation: a study of global and local optimization approaches, The Visual Computer 20 (8) (2004) 521–539. [doi:10.1007/s00371-004-0256-0](https://doi.org/10.1007/s00371-004-0256-0).
- [12] A. Jung, S. Hahmann, D. Rohmer, A. Begault, L. Boissieux, M.-P. Cani, Sketching folds: Developable surfaces from non-planar silhouettes, ACM Trans. Graph. 34 (5) (2015) 155:1–155:12. [doi:10.1145/2749458](https://doi.org/10.1145/2749458).
- [13] P. Decaudin, D. Julius, J. Wither, L. Boissieux, A. Sheffer, M.-P. Cani, Virtual garments: A fully geometric approach for clothing design, Computer Graphics Forum 25 (3) (2006) 625–634. [doi:10.1111/j.1467-8659.2006.00982.x](https://doi.org/10.1111/j.1467-8659.2006.00982.x).
- [14] Y. Liu, H. Pottmann, J. Wallner, Y.-L. Yang, W. Wang, Geometric modeling with conical meshes and developable surfaces, ACM Transactions on Graphics 25 (3) (2006) 681–689. [doi:10.1145/1141911.1141941](https://doi.org/10.1145/1141911.1141941).
- [15] J. Solomon, E. Vouga, M. Wardetzky, E. Grinspun, Flexible developable surfaces, Computer Graphics Forum 31 (5) (2012) 1567–1576, proc. Symposium Geometry Processing. [doi:10.1111/j.1467-8659.2012.03162.x](https://doi.org/10.1111/j.1467-8659.2012.03162.x).
- [16] M. Rabinovich, T. Hoffmann, O. Sorkine-Hornung, Discrete geodesic nets for modeling developable surfaces, ACM Transactions on Graphics 37 (2) (2018) 16:1–16:17. [doi:10.1145/3180494](https://doi.org/10.1145/3180494).
- [17] M. Rabinovich, T. Hoffmann, O. Sorkine-Hornung, The shape space of discrete orthogonal geodesic nets, ACM Transactions on Graphics 37 (6) (2018) 228:1–228:17.
- [18] F. Pérez, J. A. Suárez, Quasi-developable B-spline surfaces in ship hull design, Computer-Aided Design 39 (10) (2007) 853 – 862. [doi:10.1016/j.cad.2007.04.004](https://doi.org/10.1016/j.cad.2007.04.004).
- [19] M. Chen, K. Tang, A fully geometric approach for developable cloth deformation simulation, The Visual Computer 26 (6) (2010) 853–863. [doi:10.1007/s00371-010-0467-5](https://doi.org/10.1007/s00371-010-0467-5).
- [20] D. Julius, V. Kraevoy, A. Sheffer, D-charts: Quasi-developable mesh segmentation, Computer Graphics Forum 24 (3) (2005) 581–590, Proc. of Eurographics. [doi:10.1111/j.1467-8659.2005.00883.x](https://doi.org/10.1111/j.1467-8659.2005.00883.x).

- [21] H. Yamauchi, S. Gumhold, R. Zayer, H.-P. Seidel, Mesh segmentation driven by Gaussian curvature, *The Visual Computer* 21 (8) (2005) 659–668. [doi:10.1007/s00371-005-0319-x](https://doi.org/10.1007/s00371-005-0319-x).
- [22] R. Narain, T. Pfaff, J. F. O’Brien, Folding and crumpling adaptive sheets, *ACM Transactions on Graphics* 32 (4) (2013) 51:1–51:8, Proc. SIGGRAPH. [doi:10.1145/2461912.2462010](https://doi.org/10.1145/2461912.2462010).
- [23] C. C. L. Wang, Y. Wang, M. M.-F. Yuen, On increasing the developability of a trimmed NURBS surface, *Engineering with Computers* 20 (1) (2004) 54–64. [doi:10.1007/s00366-004-0272-8](https://doi.org/10.1007/s00366-004-0272-8).
- [24] O. Stein, E. Grinspun, K. Crane, Developability of triangle meshes, *ACM Transactions on Graphics* 37 (4), Proc. SIGGRAPH.
- [25] H. Pottmann, M. Eigensatz, A. Vaxman, J. Wallner, Architectural geometry, *Computers and Graphics* 47 (2015) 145–164. [doi:<http://dx.doi.org/10.1016/j.cag.2014.11.002>](http://dx.doi.org/10.1016/j.cag.2014.11.002).
- [26] M. Eigensatz, M. Kilian, A. Schiftner, N. Mitra, H. Pottmann, M. Pauly, Paneling architectural freeform surfaces, *ACM Transactions on Graphics* 29 (4) (2010) 45:1–45:10, Proc. SIGGRAPH. [doi:10.1145/1778765.1778782](https://doi.org/10.1145/1778765.1778782).
- [27] H. Pottmann, A. Schiftner, P. Bo, H. Schmiedhofer, W. Wang, N. Baldassini, J. Wallner, Freeform surfaces from single curved panels, *ACM Transactions on Graphics* 27 (3) (2008) 76:1–76:10, Proc. SIGGRAPH. [doi:10.1145/1360612.1360675](https://doi.org/10.1145/1360612.1360675).
- [28] A. Schiftner, M. Eigensatz, M. Kilian, G. Chinzi, Large scale double curved glass facades made feasible – the Arena Corinthians west facade, in: Glass Performance Days Finland (Conference Proceedings), 2013, pp. 494 – 498.
- [29] D. Shelden, Digital surface representation and the constructibility of Gehry’s architecture, Ph.D. thesis, M.I.T. (2002).
- [30] M. Schneider, P. Mehrtens, Cladding freeform surfaces with curved metal panels – a complete digital production chain, in: Advances in Architectural Geometry 2012, Springer, 2013, pp. 237–242. [doi:10.1007/978-3-7091-1251-9_19](https://doi.org/10.1007/978-3-7091-1251-9_19).
- [31] E. Cerdà, L. Mahadevan, J. M. Pasini, The elements of draping, *Proceedings of the National Academy of Sciences* 101 (7) (2004) 1806–1810. [doi:10.1073/pnas.0307160101](https://doi.org/10.1073/pnas.0307160101).
- [32] R. Farouki, Pythagorean-Hodograph Curves: Algebra and Geometry Inseparable, Springer, 2008. [doi:10.1007/978-3-540-73398-0](https://doi.org/10.1007/978-3-540-73398-0).
- [33] A. Vavpetič, E. Žagar, A general framework for the optimal approximation of circular arcs by parametric polynomial curves, *Journal of Computational and Applied Mathematics* 345 (2019) 146 – 158. [doi:10.1016/j.cam.2018.06.020](https://doi.org/10.1016/j.cam.2018.06.020).
- [34] T. W. Dubé, The structure of polynomial ideals and Gröbner bases, *SIAM Journal on Computing* 19 (4) (1990) 750–773. [doi:10.1137/0219053](https://doi.org/10.1137/0219053).
- [35] L. Piegl, W. Tiller, The NURBS Book, 2nd Edition, Springer, 1997. [doi:10.1007/978-3-642-59223-2](https://doi.org/10.1007/978-3-642-59223-2).
- [36] H. Pottmann, S. Leopoldseder, M. Hofer, Registration without ICP, *Computer Vision and Image Understanding* 95 (1) (2004) 54–71. [doi:10.1016/j.cviu.2004.04.002](https://doi.org/10.1016/j.cviu.2004.04.002).
- [37] W. Wang, H. Pottmann, Y. Liu, Fitting B-spline curves to point clouds by curvature-based squared distance minimization, *ACM Transactions on Graphics* 25 (2) (2006) 214–238. [doi:10.1145/1138450.1138453](https://doi.org/10.1145/1138450.1138453).
- [38] M. Muja, D. G. Lowe, Scalable nearest neighbor algorithms for high dimensional data, *IEEE Transactions on Pattern Analysis and Machine Intelligence* 36 (2014) 2227 – 2240.
- [39] J. Nocedal, S. Wright, Numerical Optimization, Springer Series in Operations Research and Financial Engineering, Springer, 2006. [doi:10.1007/978-0-387-40065-5](https://doi.org/10.1007/978-0-387-40065-5).

- [40] Y. Liu, H. Pottmann, W. Wang, Constrained 3D shape reconstruction using a combination of surface fitting and registration, Computer-Aided Design 38 (6) (2006) 572 – 583. [doi:
https://doi.org/10.1016/j.cad.2006.01.014](https://doi.org/10.1016/j.cad.2006.01.014).
- [41] H. Pottmann, T. Randrup, Rotational and helical surface approximation for reverse engineering, Computing 60 (4) (1998) 307–322. [doi:
10.1007/BF02684378](https://doi.org/10.1007/BF02684378).